HHS Public Access

Author manuscript

Brain. Author manuscript; available in PMC 2015 June 04.

Published in final edited form as:

Brain. 2007 November ; 130(0 11): 2858–2867. doi:10.1093/brain/awm217.

Thalamic metabolism and symptom onset in preclinical Huntington's disease

A. Feigin[1,2], **C. Tang**[1,2], **Y. Ma**[1,2], **P. Mattis**[1,3], **D. Zgaljardic**[4], **M. Guttman**[5], **J. S. Paulsen**[6], **V. Dhawan**[1,2], and **D. Eidelberg**[1,2]

[1]Center for Neurosciences, The Feinstein Institute for Medical Research, North Shore-Long Island Jewish Health System, Manhasset, NY

[2]Department of Neurology, North Shore University Hospital and New York University School of Medicine, New York

[3]Department of Psychiatry, North Shore-Long Island Jewish Health System, Manhasset, NY

[4]Department of Neuropsychology, Transitional Learning Centre, Galveston, TX, USA

[5]Department of Neurology, University of Toronto, Toronto, Canada

[6]Department of Neurology, University of Iowa, Des Moines, IA, USA

Abstract

The neural basis for the transition from preclinical to symptomatic Huntington's disease (HD) is unknown. We used serial positron emission tomography (PET) imaging in preclinical HD gene carriers (p-HD) to assess the metabolic changes that occur during this period. Twelve p-HD subjects were followed longitudinally with [^{11}C]-raclopride and [^{18}F]-fluorodeoxyglucose PET imaging, with scans at baseline, 18 and 44 months. Progressive declines in striatal D_2-receptor binding were correlated with concurrent changes in regional metabolism and in the activity of an HD-related metabolic network. We found that striatal D_2 binding declined over time ($P<0.005$). The activity of a reproducible HD-related metabolic covariance pattern increased between baseline and 18 months ($P<0.003$) but declined at 44 months ($P<0.04$). These network changes coincided with progressive declines in striatal and thalamic metabolic activity ($P<0.01$). Striatal metabolism was abnormally low at all time points ($P<0.005$). By contrast, thalamic metabolism was elevated at baseline ($P<0.01$), but fell to subnormal levels in the p-HD subjects who developed symptoms. These findings were confirmed with an MRI-based atrophy correction for each individual PET scan. Increases in network expression and thalamic glucose metabolism may be compensatory for early neuronal losses in p-HD. Declines in these measures may herald the onset of symptoms in gene carriers.

Correspondence to: Dr David Eidelberg, Center for Neurosciences, The Feinstein Institute for Medical Research, North Shore-Long Island Jewish Health System, 350 Community Drive, Manhasset, NY11030, USA, david1@nshs.edu.

Keywords

preclinical Huntington's disease (p-HD); brain metabolism; positron emission tomography (PET)

Introduction

Huntington's disease (HD) is an autosomal dominant neurodegenerative disorder that results in progressive impairments in cognition, motor function and behaviour (Feigin and Zgaljardic, 2002). On average, the disease begins in middle adulthood and progresses to death over approximately 20 years (Anderson, 2005). However, both age of onset and rate of progression vary widely (Kieburtz *et al*., 1994; Feigin *et al*., 1995). Recent advances in understanding the pathophysiology of HD have led to new approaches to neuroprotective therapies aimed at slowing the progression of disease or forestalling onset.

Among neurodegenerative diseases, HD is unique in that individuals destined to develop symptoms can be identified through genetic testing before clinical signs of the disease begin. This raises the possibility of directing therapies toward preventing or delaying disease onset. Currently, clinical measures remain the gold standard for assessing disease progression in this and other neurodegenerative diseases. Nonetheless, in the preclinical period, clinical measures such as the Unified Huntington's Disease Rating Scale (UHDRS) are insensitive to disease progression. However, MRI and positron emission tomography (PET) studies have demonstrated that the degenerative process precedes the onset of clinical signs by years (Aylward *et al*., 1996; Antonini *et al*., 1998; Aylward *et al*., 2000; Paulsen *et al*., 2004). Two large multicenter studies (Biglan and Investigators, 2004; Ross *et al*., 2004) are currently underway to determine how clinical trials in preclinical HD (p-HD) could be powered if clinical onset were utilized as an endpoint.

Utilizing ^{18}F-fluorodeoxyglucose (FDG) and PET, we have previously used a network approach to identify a unique spatial covariance pattern in preclinical HD subjects and in patients with early symptomatic HD (Feigin *et al*., 2001). In that study we found that the expression of this HD-related metabolic covariance pattern (HDRP) was abnormally elevated in p-HD subjects, with yet greater increases in network expression in symptomatic individuals. In the current investigation, we validated the HDRP topography in an independent p-HD cohort using newer network mapping techniques. We then followed these subjects longitudinally to assess changes in HDRP activity over time. In addition to monitoring the development of metabolic abnormalities in preclinical subjects, we also assessed concurrent changes in striatal D_2 neuroreceptor binding using ^{11}C-raclopride (RAC) and PET. We chose to measure RAC binding because it has been widely used in HD and has been documented to decline over time in p-HD (Antonini *et al*., 1996, 1998; Pavese *et al*., 2003); in addition, declines in D_2 receptors are among the earliest manifestations of HD pathology likely through transcriptional inhibition (Dunah *et al*., 2002). The results pointed to the loss of a thalamic compensatory mechanism in the p-HD subjects who developed clinical manifestations in the course of the 4-year follow-up period.

Materials and methods

Subjects

Twelve p-HD gene carriers [age 46.8±11.0 (mean±SD); cytosine, adenine, guanine (CAG) repeat length 41.6±1.7; estimated years-to-onset (Langbehn *et al*., 2004; Feigin *et al*., 2006) 10.3±8.6] underwent FDG and RAC imaging, as well as MRI and clinical assessments. Two sets of control subjects were utilized as reference groups for the PET scans, one for the FDG (n = 12; age 40.8±14.7) and one for the RAC (n = 11; age 41.5±16.1) PET scans. All p-HD subjects had undergone genetic testing prior to entry into this study and were known to have CAG expansions $\geqslant$39. Specific CAG repeat information was available for 11 of the subjects; one subject declined to provide CAG repeat number because of concern regarding confidentiality. The subjects were evaluated by a neurologist (A.F.) experienced with HD, and were felt not to have sufficient neurological signs to be diagnosed with HD at baseline. None of the subjects were treated with psychoactive medications. At follow-up visits all clinical information (motor, behavioural, cognitive and functional) was utilized to determine if subjects could be diagnosed with definite HD. Ethical permission for these studies was obtained from the Institutional Review Board of North Shore University Hospital. Written informed consent was obtained from each subject following detailed explanation of the procedures.

Clinical evaluations

Study evaluations were performed at baseline and following 18±1 and 44±4 months. At each time point, the subjects were evaluated according to the UHDRS (Huntington Study Group, 1996). They also underwent a comprehensive neuropsychological battery that included the following tests: Dementia Rating Scale (Mattis, 1988), estimated IQ (Nelson, 1982), Beck Depression Inventory (Beck, 1987), Stroop Interference Test (Goldon, 1978), Symbol Digit Modalities Test (Smith, 1982), Integrated Visual and Auditory Continuous Performance Test (IVA) (Sandford and Turner, 1995) and Trail Making A and B (Army Individual Test Battery, 1944).

Positron emission tomography

All p-HD subjects underwent PET imaging with both RAC and FDG at baseline and at subsequent visits; scanning with the two radiotracers was performed over a 2-day period. Subjects fasted overnight prior to each imaging session. The PET studies were performed in three-dimensional mode using the GE Advance tomograph at North Shore University Hospital. This 8-ring bismuth germanate scanner provided 35 two-dimensional image planes with an axial field of view of 14.5 cm and transaxial resolution of 4.2mm (FWHM) in all directions. The scans were performed with the subject's eyes open in a dimly lit room and with minimal auditory stimulation. Subjects were positioned in the scanner using a stereoadapter (Sandstrom Trade and Technology, Inc; Welland, Ontario, Canada) (Laitinen *et al*., 1985) with three-dimensional laser alignment with reference to the orbitomeatal line; identical stereoadapter and laser settings were used in each imaging session.

Data analysis

Striatal D_2 receptor binding—Dynamic RAC PET scans were acquired over 70 min (7×10 min), as described previously (Asanuma *et al*., 2005). The individual frames were spatially realigned to compensate for potential movement during scanning. All images involving the striatum were integrated into a single slice for region-of-interest (ROI) analysis. ROIs were placed bilaterally on the caudate nucleus, putamen and the occipital cortex blind to subject identity, CAG repeat length, and time point (Kazumata *et al*., 1998). At each time point, D_2 receptor binding affinity was estimated for the caudate and putamen by the distribution volume ratio over 30–60 min following injection using a Logan plot (Logan, 2000). For each ROI, left and right values were averaged and compared with analogous values for the RAC control group.

Longitudinal changes in caudate and putamen RAC binding over time were analysed with one-way repeated measures analysis of variance (RMANOVA) performed on the data acquired at all three time points. This was performed using an iterative method to fit a mixed model (Searle *et al*., 1992; Underwood *et al*., 2006). *Post-hoc* comparisons were performed between time points (e.g., 2–1, 3–2, 3–1) using Tukey's HSD test.

Regional metabolism and spatial covariance analysis—FDG PET was used to quantify rates of glucose metabolism on a voxel-by-voxel basis employing a single arterial sampling technique (Takikawa *et al*., 1993). Arterial plasma input function was derived from a previously established population input function scaled by the individuals' single arterial blood sample taken at 15–20 min post FDG injection. To identify metabolic patterns associated with HD carrier status, we analysed the metabolic images using a voxel-based network modelling approach. This method is based on principal components analysis (PCA) and can be used to detect genotype-specific spatial covariance patterns in mutation carriers (Feigin *et al*., 2001; Trošt *et al*., 2002). In this study, we used an automated software package available at our website (http://www.feinsteinneuroscience.org/software) to rapidly perform PCA on groups of brain images transformed into a common anatomical space.

To delineate topographies associated with p-HD, we performed a combined group analysis of the baseline FDG PET scans of the 12 p-HD subjects and the 12 FDG control subjects. We limited the analysis to the first and second principal components (PCs), or a linear combination of the two (Moeller *et al*., 1999). The resulting covariance patterns were considered to be p-HD-related if the associated subject scores (PC scalars) distinguished gene carriers from controls at a threshold of $P<0.01$. Voxel weights at the local maxima were Z-thresholded at 2.44, corresponding to significant ($P\leq0.01$) contributions to whole brain network activity at peak voxel, and further tested for reliability using a bootstrap resampling procedure (Efron and Tibshirani, 1994). Coordinates were reported in the standard anatomical space developed at the Montreal Neurological Institute (Collins *et al*., 1994).

For each subject, we quantified the expression of the HDRP at baseline and at the subsequent two time points. This was accomplished using an automated single scan routine described in detail elsewhere (Spetsieris *et al*., 2006; Ma *et al*., 2007). These computations were performed blind to subject, CAG repeat length and time point. Network expression was

also quantified in the 12 normal controls. Subject scores for the entire cohort (HD subjects and healthy controls) were *z*-transformed and adjusted so that the mean of the control group was zero. Changes in HDRP expression were assessed with RMANOVA across time points as described above. To examine the trajectory of longitudinal change in HDRP expression, we used an individual growth curve model (Singer and Willett, 2003) to fit the data. These calculations were performed using SAS (Singer, 1998). Changes in HDRP were correlated with concurrent changes in striatal D_2 receptor binding by computing the Bland–Altman within-subject correlation coefficient (Bland and Altman, 1995). To identify factors that might predict the rate of progression, we correlated the observed changes in caudate/putamen RAC binding with the following baseline subject descriptors: (1) age at the time of the study; (2) CAG repeat length; (3) predicted years-to-onset (Langbehn *et al*., 2004; Feigin *et al*., 2006); (4) baseline UHDRS motor score; and (5) baseline weight. In these correlations, changes in HDRP expression and RAC binding were determined by calculating individual subject differences between time points 1 and 3 and dividing by the time between scans. All correlational analyses were considered significant for $P<0.05$.

Lastly, we assessed the time course of the metabolic changes within each of the major regions that comprise the HDRP network. In each network region we identified the voxel for which metabolism had the greatest difference between the baseline p-HD and the control scans. The coordinates of this voxel were determined with statistical parametric mapping (Wellcome Department of Cognitive Neurology, London, UK) with a threshold of $T>3.53$, $P<0.001$ (uncorrected). Metabolic activity in each region was measured within a sphere (r = 4mm) centred on the peak voxel; the same volume-of-interest (VOI) was analysed at each of the three time points. To account for inter-individual variability in global metabolic rate, each VOI measure was ratio normalized by the global metabolic rate. These values were plotted and displayed with respect to reference values from the control subjects (see above). Longitudinal changes in the regional measures were assessed with RMANOVA followed by *post-hoc* testing as described above. In areas found to decline significantly with time, we excluded the effects of progressive local volume loss using an MRI-based atrophy correction determined for each PET scan (Ma *et al*., 2003; Feigin *et al*., 2006). Lastly, the mean change at each node in the four subjects, who converted to symptomatic HD was graphically compared with that in those who remained preclinical during the course of the study.

Results

Clinical characteristics

Baseline total UHDRS motor scores were 9.6±11.8; and these did not change after 18 months (9.3±10.8; $P = 0.9$) or 44 months (10.1±13.8; $P = 0.6$). UHDRS motor scores at baseline correlated with the predicted years-to-onset ($r = 0.66$; $P<0.03$). Additional baseline UHDRS sub-scores were as follows: behavioural 9.5±10.1, independence scale 100±0, total functional capacity 12.9±0.3. At baseline, three subjects were classified as probably showing signs of HD (UHDRS item # 17 = 3). At 18 months, two of these subjects were diagnosed with definite HD; at 44 months, two additional subjects were diagnosed with HD (all three subjects with subtle signs of HD at baseline were ultimately diagnosed). The subjects' average weight increased from 175±36 to 196±39 pounds ($P = 0.1$) over 18 months. At 44

months, weight had begun to decline (183±32; $P = 0.3$ compared to time point 2) likely indicating the increasing number of p-HD subjects at or near the point of symptom onset.

Baseline neuropsychological testing was normal (e.g. Dementia Rating Scale 139.3±4.2, estimated IQ 111.6±8.9, Beck Depression Inventory 3.8±5.0, Stroop Interference 55.8±7.7, Symbol Digit 58.8±16.3, IVA Visual 47.1±11.0 and Auditory 44.7±18.5, Trail Making A 29.7±9.6 and B 63.0±10.8). These measures did not change over the course of the study ($P>0.68$). At baseline, Stroop Interference performance correlated with the predicted years-to-onset ($r = -0.65$; $P<0.03$). Interestingly, age at the beginning of the study correlated negatively with CAG repeat length ($r = 0.66$; $P<0.03$), likely reflecting the fact that young p-HD subjects on average have longer CAG repeat lengths than older p-HD subjects (p-HD subjects with long CAG repeat lengths are less likely to remain presymptomatic with advanced age).

D_2 receptor binding

Over the course of the study, caudate and putamen RAC binding declined from a baseline of 2.55±0.33 (mean±SD) and 2.52±0.33 (corresponding to 82% and 80% of the normal mean, respectively), to 2.36±0.20 and 2.33±0.26 (76% and 74% of the normal mean) at 18 months ($P<0.03$, with respect to baseline). These values continued to decline to 2.27±0.25 and 2.21±0.26 (73% and 70% of the normal mean) at 44 months ($P<0.001$, with respect to baseline). There was a significant effect of time across time points for both caudate ($F_{2,18} = 7.19$, $P<0.006$) and putamen ($F_{2,18} = 8.46$, $P<0.004$). Predicted years-to-onset correlated with baseline striatal RAC binding ($r = 0.69$; $P<0.03$), but not with the rate of decline in RAC binding over time. None of the other baseline clinical or imaging measures predicted the rate of decline in RAC binding.

Network analysis

Voxel-based network analysis of the baseline FDG PET scans from the combined group of the p-HD subjects and controls ($n = 24$) revealed the presence of a significant spatial covariance pattern that discriminated the gene carriers from the controls ($P<0.01$). This HD-related pattern (HDRP) was represented by the first principal component (PC1), accounting for 18% of the subject × voxel variance. This pattern (Fig. 1; Table 1) was characterized by reductions in striatal and anterior cingulate metabolic activity, associated with relative metabolic increases in the ventrolateral (VL)/ventral posterolateral (VPL) thalamus, cerebellar vermis and in the primary motor and visual regions of the cerebral cortex. Region weights for this HDRP were found to be stable on bootstrap resampling ($P<0.001$), and were highly correlated ($R^2 = 0.77$, $P<0.001$) with those reported by us previously (Feigin *et al.*, 2001) in the network analysis of a different p-HD cohort.

HDRP expression increased significantly ($P<0.003$) over the first 18 months of follow-up, but declined at 44 months ($P<0.04$, compared to time point 2; Fig. 2). There was a significant effect of time across time points ($F_{2,20} = 5.98$, $P<0.01$; RMANOVA). The initial increase and subsequent decline in HDRP expression conformed to a quadratic [curvilinear] model ($P<0.001$). Despite the observed decline between the second and third time points, HDRP expression at 44 months remained elevated with respect to controls ($P<0.01$).

Interestingly, we found that baseline network expression was higher in those p-HD subjects who subsequently phenoconverted (Fig. 2, triangles). Indeed, network expression correlated with estimated years-to-onset at each of the three time points (R^2>0.43, P<0.03). Changes in HDRP expression over all three time points did not correlate with changes in caudate or putamen RAC binding. As noted above, HDRP expression initially increased and then declined, while RAC binding steadily declined.

To investigate the mechanism of the decline in HDRP expression at 44 months, we analysed the time course of the changes in regional activity at each of the major nodes of this metabolic network. At baseline, regional metabolism in the p-HD subjects was reduced relative to controls in the caudate and putamen (P<0.005), and in the cingulate cortex (P<0.0001) (Fig. 3A, B; Table 2). By contrast, regional metabolism was elevated at baseline in the VL and mediodorsal (MD) thalamic nuclei (P<0.01), and in the cerebellum (P<0.001) (Fig. 3C, D; Table 2). Over the course of the study, regional metabolism progressively declined in the striatum ($F_{2, 20}$ = 7.36, P<0.005; RMANOVA), and in the thalamus ($F_{2, 20}$ = 6.03, P<0.01) (Fig. 3A, C). Longitudinal changes in these regions remained significant following atrophy correction (caudate/putamen: P<0.03; thalamus: P<0.005). Interestingly, clinical phenoconversion was associated with a decline in normalized thalamic metabolic activity to values below the normal mean (Fig. 3, open triangles). Elevations in thalamic metabolism were sustained in the subgroup of gene carriers who did not develop signs of HD during the course of the study.

Discussion

Preclinical HD represents a unique therapeutic opportunity among neurodegenerative disorders, in that future patients can be identified and potentially treated to delay or prevent the onset of clinical symptoms. In order to assess the efficacy of therapies in the preclinical phase of the illness, biomarkers are needed that accurately reflect the progression of disease. In this study, we have applied a voxel-based network mapping approach to identify an abnormal pattern of brain metabolism in p-HD subjects. Indeed, its spatial topography was highly correlated with a metabolic pattern that we had previously described in a separate population of preclinical carriers (Feigin *et al*., 2001). In addition, we found that network expression increases over time in the early preclinical phase of the disease, but begins to decline as HD gene carriers approach symptom onset. Furthermore, network expression correlated with predicted years to symptom onset as determined by the subjects' CAG repeat length and age. Indeed, p-HD carriers with elevated HDRP scores at baseline were more likely to convert to symptomatic HD over a 3-year follow-up period than those with baseline HDRP expression in the normal range (3/5 for scores $\geqslant$1.5 versus 1/7 for scores in the normal range; see Fig. 2). These observations suggest that this functional measure has biological significance.

The HDRP metabolic network likely represents a combination of anatomical cell loss, downstream changes in brain circuitry and compensatory changes. Widespread brain volume changes occur in p-HD, including subcortical and cortical decreases (Rosas *et al*., 2002, 2004) and increases (Paulsen *et al*., 2006). These structural changes are likely to contribute to the local and network-wide changes that were recorded with PET. Nonetheless, when we

performed an atrophy correction on the scan data, there was little change in the time course of disease progression at either the network or regional level (Ma *et al*., 2003). Indeed, the non-linear trajectory of HDRP progression in the preclinical period raises the possibility that adaptive/compensatory processes are active prior to symptom onset. To explore this possibility, we analysed the time course of changes in regional metabolism within key nodes of the HDRP network. We found that striatal activity was abnormally low throughout the duration of the study, with relatively greater declines in the p-HD subjects who subsequently phenoconverted during the 44 months of observation. Interestingly, significant elevations in thalamic metabolism, localized to the VL and MD nuclei, were evident in the baseline scans of the p-HD subjects. Whereas increased levels of thalamic metabolic activity were sustained in the non-converters, a progressive loss of this compensatory response was observed in the p-HD subjects who proceeded to phenoconvert. Given that only four subjects phenoconverted during the course of our study, our observations will need to be confirmed in a larger cohort.

We have recently reported increased thalamic activation in this group of p-HD subjects during the performance of a motor learning task (Feigin *et al*., 2006). Based upon the results of both studies, we hypothesize that increasing thalamic activity, at rest and during task performance, may compensate for the loss of striato-cortical activity in the very early preclinical period. The mechanism underlying the observed thalamic response to progressive dysfunction and/or loss of striatal projection neurons is unknown, although positive feedback from the intralaminar thalamic nuclei to the striatum is possible (Smith *et al*., 2004). As the disease progresses to include thalamic neuronal loss (Sotrel *et al*., 1991; Heinsen *et al*., 1996, 1999; Kassubek *et al*., 2005; Paulsen *et al*., 2006), this compensatory mechanism diminishes and the symptoms of HD begin to emerge. Metabolic decline in the VL thalamus is also likely to reflect an ongoing loss of inhibitory pallidothalamic output (Eidelberg *et al*., 1997). The hypothesis based upon our data regarding the time course of the regional metabolic changes in early HD is presented in Fig. 4.

We also found abnormally reduced metabolism in the cingulate cortex in p-HD, as well as elevated metabolism in the cerebellum. The cingulate has been found to be involved in HD both functionally (Mayberg *et al*., 1992; Reading *et al*., 2004) and as a locus of primary cell loss (Pavese *et al*., 2006). The cerebellar hypermetabolism that we observed was greater in the p-HD subjects who ultimately phenoconverted. However, unlike thalamic hypermetabolism, metabolic activity in the cerebellum increased further as subjects phenoconverted, suggesting that this functional abnormality may emerge as chorea develops.

Several lines of evidence suggest that abnormal cellular metabolism may be a feature of the neuropathological process underlying HD. Non-neuronal tissues demonstrate metabolic impairments in HD patients (Lodi *et al*., 2000; Saft *et al*., 2005), and in brain, increases in lactate levels have been demonstrated utilizing MR spectroscopy (Koroshetz *et al*., 1997). Multiple biochemical studies have identified abnormalities in mitochondrial electron transport in HD (Gu *et al*., 1996; Browne *et al*., 1997; Tabrizi *et al*., 1999), and mitochondrial toxins can induce selective neurodegeneration in animal models that mimic HD neuropathology (Brouillet *et al*., 2005). In transgenic animal models of HD, CAG repeat

length correlates with striatal metabolic rates (Jenkins *et al*., 2005), and perhaps most relevant to our study is a recent observation that brain metabolism initially increases before neurodegeneration leads to regional hypometabolism (M.F. Beal and S. Browne, unpublished data). Similar to our findings, in the transgenic model, hypermetabolism is not restricted to the brain regions primarily affected in HD. Though our data suggests that the hypermetabolism observed in VL thalamus and cerebellum may be compensatory in nature, it may also be possible that this is simply heralding impending metabolic failure and cell death. Further studies will be needed to evaluate whether hypermetabolism precedes the onset of neurodegeneration in other brain regions, including the striatum.

We also found that striatal D_2 receptor binding declined steadily in p-HD, due presumably to progressive down-regulation of receptor expression and the loss of receptor-bearing projection neurons. In fact, decreased striatal D_2 receptor expression may be one of the earliest physiological manifestations of HD, which may relate to transcriptional dysregulation induced by the CAG repeat expansion (Augood *et al*., 1997; Cha *et al*., 1999). Longitudinal changes in striatal D_2 receptor binding however do not correlate with HDRP expression, as the latter initially increases and then declines. It is also worth noting that HDRP and RAC are better at predicting time to onset as p-HD subjects approach disease onset. Correlations of these measures with predicted years-to-onset were better at time point 2 than at baseline, suggesting that the further a subject is from HD onset, the greater the variability in both imaging measures.

We found that significant progression of imaging measures occurred at a time when there were no changes in motor UHDRS ratings. Specifically, HDRP expression initially increased by 40%, and striatal RAC binding declined by approximately 10% over the course of the study. These findings are consistent with a recent MRI study that found cerebral volume changes in p-HD that occurred in the absence of clinical changes (Kipps *et al*., 2005). Indeed, these observations suggest that imaging may be useful for measuring progression of HD before clinical onset. Nonetheless, future studies will need to examine the acute and subacute effects of drugs on HDRP expression and RAC binding, as this could represent a significant confound for measuring disease progression, as has been recently demonstrated in Parkinson's disease (Feigin, 2004). In the present study, none of the subjects were on central nervous system active drugs.

Finally, one surprising result of our study was the observation that baseline motor UHDRS scores and neuropsychological tests of executive function (Stroop Interference) correlated with predicted years to disease onset. This suggests that subtle motor and cognitive changes in the preclinical phase of the illness have significance and are at least in part caused by HD pathological changes. In the plot of UHDRS against predicted years-to-onset, if we extrapolate back to when UHDRS scores would be zero, we estimate that subtle clinical signs of HD may begin to emerge approximately 12.2 years before HD is diagnosed (95% CI 2.9–21.6 years). Similar calculations for the plots of striatal D_2 receptor binding, striatal regional metabolism and HDRP network expression predict that these measures begin, respectively, to worsen at 24.9 years (95% CI 12.3–37.6 years), 19.8 years (95% CI 13.8–25.8 years) and 14.7 years (95% CI 8.7–20.8 years) before HD diagnosis (Fig. 4). Though UHDRS scores and neuropsychological tests in p-HD are meaningful, our findings

nonetheless suggest that, unlike brain metabolism (including HDRP) and striatal dopamine D_2 receptor binding, these clinical measures may not be sensitive to progression in p-HD, in that in our study, these did not change over the 44 months of observation.

In conclusion, p-HD is characterized by a unique pattern of brain metabolism that is present in two independent cohorts of preclinical gene carriers. The current longitudinal study shows that PET imaging with either FDG or RAC can detect significant changes over as little as 1.5 years in a relatively small cohort of p-HD subjects. Moreover, the measured changes likely have a biological basis in experimental models of the HD neurodegenerative process. Furthermore, as previously reported (van Oostrom *et al*., 2005), we found that changes in brain metabolism and dopamine D_2 receptor binding appear to precede significant volumetric changes. Our findings indicate that different clinical and imaging descriptors may be more useful for following progression during different phases of the disease. For example, in the very early preclinical period, HDRP network expression and local striatal measures of glucose utilization or D_2 receptor binding may each be helpful, while UHDRS would not. As subjects move closer to disease onset, the UHDRS may become more useful, and declines in thalamic metabolism may predominate. However, at this time the local striatal measures, as well as the HDRP scores, may become relatively insensitive to disease progression. Unlike HDRP, D_2 receptor binding appears to decline steadily throughout the presymptomatic period, and may therefore be a useful descriptor of progression during this phase of disease. Future studies targeting young HD gene carriers will be needed to determine when the earliest brain changes can be identified.

Acknowledgments

This research project was funded by NIH RO1 NS 37564 and the Susan and Leonard Feinstein Center for the Neurosciences at The Feinstein Institute for Medical Research, North Shore-Long Island Jewish Health System. Dr A. Feigin was funded by K08 NS 02011 and the Huntington's Disease Society of America and Dr D. Eidelberg by K24 NS 02101. Dr Paulsen was funded by NIMH 01579, Roy J. Carver Trust Medicine Research Initiative, and Howard Hughes Medical Institute. Special thanks to Ms Toni Flanagan for manuscript preparation.

Abbreviations

BA	Brodmann area
FDG	^{18}F-fluorodeoxyglucose
HD	Huntington's disease
HDRP	HD-related metabolic covariance pattern
IVA	integrated visual and auditory continuous performance test
MD	mediodorsal
PCA	principal components analysis
PC1	first principal component
PCs	principal components
PET	positron emission tomography

p-HD	preclinical Huntington's disease
RAC	^{11}C-raclopride
RMANOVA	repeated measures analysis of variance
ROI	region-of-interest
UHDRS	unified Huntington's disease rating scale
VL	ventrolateral
VOI	volume-of-interest
VPL	ventrolateral posterolateral

References

Anderson KE. Huntington's disease and related disorders. Psychiatr Clin North Am. 2005; 28:275–90. [PubMed: 15733623]

Antonini A, Leenders KL, Eidelberg D. [11C]raclopride-PET studies of the Huntington's disease rate of progression: relevance of the trinucleotide repeat length. Ann Neurol. 1998; 43:253–5. [PubMed: 9485067]

Antonini A, Leenders KL, Spiegel R, Meier D, Vontobel P, Weigell-Weber M, et al. Striatal glucose metabolism and dopamine D2 receptor binding in asymptomatic gene carriers and patients with Huntington's disease. Brain. 1996; 119:2085–95. [PubMed: 9010012]

Army Individual Test Battery. Manual of Directions and Scoring. Washington, DC: War Department, Adjutant General's Office; 1944.

Asanuma K, Ma Y, Okulski J, Dhawan V, Chaly T, Carbon M, et al. Decreased striatal D2 receptor binding in non-manifesting carriers of the DYT1 dystonia mutation. Neurology. 2005; 64:347–9. [PubMed: 15668438]

Augood SJ, Faull RL, Emson PC. Dopamine D1 and D2 receptor gene expression in the striatum in Huntington's disease. Ann Neurol. 1997; 42:215–21. [PubMed: 9266732]

Aylward EH, Codori AM, Barta PE, Pearlson GD, Harris GJ, Brandt J. Basal ganglia volume and proximity to onset in presymptomatic Huntington disease. Arch Neurol. 1996; 53:1293–6. [PubMed: 8970459]

Aylward EH, Codori AM, Rosenblatt A, Sherr M, Brandt J, Stine OC, et al. Rate of caudate atrophy in presymptomatic and symptomatic stages of Huntington's disease. Mov Disord. 2000; 15:552–60. [PubMed: 10830423]

Beck, A. Beck Depression Inventory: Manual. San Antonio, TX: Psychological Corporation; 1987.

Biglan KM, Investigators P. Baseline characteristics of the prospective Huntington at risk observational study cohort. Ann Neurol. 2004; 56:S24.

Bland JM, Altman DG. Calculating correlation coefficients with repeated observations: part 1–Correlation within subjects. Br Med J. 1995; 310:446. [PubMed: 7873953]

Brouillet E, Jacquard C, Bizat N, Blum D. 3-Nitropropionic acid: a mitochondrial toxin to uncover physiopathological mechanisms underlying striatal degeneration in Huntington's disease. J Neurochem. 2005; 95:1521–40. [PubMed: 16300642]

Browne SE, Bowling AC, MacGarvey U, Baik MJ, Berger SC, Muqit MM, et al. Oxidative damage and metabolic dysfunction in Huntington's disease: selective vulnerability of the basal ganglia. Ann Neurol. 1997; 41:646–53. [PubMed: 9153527]

Cha JH, Frey AS, Alsdorf SA, Kerner JA, Kosinski CM, Mangiarini L, et al. Altered neurotransmitter receptor expression in transgenic mouse models of Huntington's disease. Philos Trans R Soc Lond B Biol Sci. 1999; 354:981–9. [PubMed: 10434296]

Collins DL, Neelin P, Peters TM, Evans AC. Automatic 3D intersubject registration of MR volumetric data in standardized Talairach space. J Comput Assist Tomogr. 1994; 18:192–205. [PubMed: 8126267]

Dunah AW, Jeong H, Griffin A, Kim YM, Standaert DG, Hersch SM, et al. Sp1 and TAFII130 transcriptional activity disrupted in early Huntington's disease. Science. 2002; 296:2238–43. [PubMed: 11988536]

Efron, B.; Tibshirani, R. An introduction to the bootstrap. New York: CRC Press, LLC; 1994.

Eidelberg D, Moeller JR, Kazumata K, Antonini A, Sterio D, Dhawan V, et al. Metabolic correlates of pallidal neuronal activity in Parkinson's disease. Brain. 1997; 120:1315–24. [PubMed: 9278625]

Feigin A. Evidence from biomarkers and surrogate endpoints. Neuro Rx. 2004; 1:323–30.

Feigin A, Ghilardi MF, Huang C, Ma Y, Carbon M, Guttman M, et al. Preclinical Huntington's disease: compensatory brain responses during learning. Ann Neurol. 2006; 59:53–9. [PubMed: 16261565]

Feigin A, Kieburtz K, Bordwell K, Como P, Steinberg K, Sotack J, et al. Functional decline in Huntington's disease. Mov Disord. 1995; 10:211–4. [PubMed: 7753064]

Feigin A, Leenders KL, Moeller JR, Missimer J, Kuenig G, Spetsieris P, et al. Metabolic network abnormalities in early Huntington's disease: an [(18)F]FDG PET study. J Nucl Med. 2001; 42:1591–5. [PubMed: 11696626]

Feigin A, Zgaljardic D. Recent advances in Huntington's disease: implications for experimental therapeutics. Curr Opin Neurol. 2002; 15:483–9. [PubMed: 12151847]

Goldon, C. Stroop Color and Word Test. Chicago: Stoelting Company; 1978.

Gu M, Gash MT, Mann VM, Javoy-Agid F, Cooper JM, Schapira AH. Mitochondrial defect in Huntington's disease caudate nucleus. Ann Neurol. 1996; 39:385–9. [PubMed: 8602759]

Heinsen H, Rub U, Bauer M, Ulmar G, Bethke B, Schuler M, et al. Nerve cell loss in the thalamic mediodorsal nucleus in Huntington's disease. Acta Neuropathol. 1999; 97:613–22. [PubMed: 10378380]

Heinsen H, Rub U, Gangnus D, Jungkunz G, Bauer M, Ulmar G, et al. Nerve cell loss in the thalamic centromedian-parafascicular complex in patients with Huntington's disease. Acta Neuropathol. 1996; 91:161–8. [PubMed: 8787149]

Huntington Study Group. Unified Huntington's Disease Rating Scale: reliability and consistency. Mov Disord. 1996; 11:136–42. [PubMed: 8684382]

Jenkins BG, Andreassen OA, Dedeoglu A, Leavitt B, Hayden M, Borchelt D, et al. Effects of CAG repeat length, HTT protein length and protein context on cerebral metabolism measured using magnetic resonance spectroscopy in transgenic mouse models of Huntington's disease. J Neurochem. 2005; 95:553–62. [PubMed: 16135087]

Kassubek J, Juengling FD, Ecker D, Landwehrmeyer GB. Thalamic atrophy in Huntington's disease co-varies with cognitive performance: a morphometric MRI analysis. Cereb Cortex. 2005; 15:846–53. [PubMed: 15459079]

Kazumata K, Dhawan V, Chaly T, Antonini A, Margouleff C, Belakhlef A, et al. Dopamine transporter imaging with fluorine-18-FPCIT and PET. J Nucl Med. 1998; 39:1521–30. [PubMed: 9744335]

Kieburtz K, MacDonald M, Shih C, Feigin A, Steinberg K, Bordwell K, et al. Trinucleotide repeat length and progression of illness in Huntington's disease. J Med Genet. 1994; 31:872–4. [PubMed: 7853373]

Kipps CM, Duggins AJ, Mahant N, Gomes L, Ashburner J, McCusker EA. Progression of structural neuropathology in preclinical Huntington's disease: a tensor based morphometry study. J Neurol Neurosurg Psychiatry. 2005; 76:650–5. [PubMed: 15834021]

Koroshetz WJ, Jenkins BG, Rosen BR, Beal MF. Energy metabolism defects in Huntington's disease and effects of coenzyme Q10. Ann Neurol. 1997; 41:160–5. [PubMed: 9029064]

Laitinen LV, Liliequist B, Fagerlund M, Eriksson AT. An adapter for computed tomography-guided stereotaxis. Surg Neurol. 1985; 23:559–66. [PubMed: 3887625]

Langbehn DR, Brinkman RR, Falush D, Paulsen JS, Hayden MR. A new model for prediction of the age of onset and penetrance for Huntington's disease based on CAG length. Clin Genet. 2004; 65:267–77. [PubMed: 15025718]

Lodi R, Schapira AH, Manners D, Styles P, Wood NW, Taylor DJ, et al. Abnormal in vivo skeletal muscle energy metabolism in Huntington's disease and dentatorubropallidoluysian atrophy. Ann Neurol. 2000; 48:72–6. [PubMed: 10894218]

Logan J. Graphical analysis of PET data applied to reversible and irreversible tracers. Nucl Med Biol. 2000; 27:661–70. [PubMed: 11091109]

Ma Y, Feigin A, Okulski J, Dhawan V, Chaly T, Eidelberg D. Implementation of atrophy correction in metabolic mapping studies of presymptomatic Huntington's disease. J Cereb Blood Flow Metab. 2003; 23:S629.

Ma Y, Tang C, Spetsieris P, Dhawan V, Eidelberg D. Abnormal metabolic network activity in Parkinson's disease: test-retest reproducibility. J Cereb Blood Flow Metab. 2007; 27:597–605. [PubMed: 16804550]

Mattis, S. Dementia Rating Scale: profressional manual. Odesa: Psychological Assessment Resources; 1988.

Mayberg HS, Starkstein SE, Peyser CE, Brandt J, Dannals RF, Folstein SE. Paralimbic frontal lobe hypometabolism in depression associated with Huntington's disease. Neurology. 1992; 42:1791–7. [PubMed: 1387463]

Moeller JR, Nakamura T, Mentis MJ, Dhawan V, Spetsieres P, Antonini A, et al. Reproducibility of regional metabolic covariance patterns: comparison of four populations. J Nucl Med. 1999; 40:1264–9. [PubMed: 10450676]

Nelson, HE. The National Adult Reading Test (NART): test manual. Windsor, Berks, UK: NFER-Nelson; 1982.

Paulsen JS, Magnotta VA, Mikos AE, Paulson HL, Penziner E, Andreasen NC, et al. Brain structure in preclinical Huntington's disease. Biol Psychiatry. 2006; 59:57–63. [PubMed: 16112655]

Paulsen JS, Zimbelman JL, Hinton SC, Langbehn DR, Leveroni CL, Benjamin ML, et al. fMRI biomarker of early neuronal dysfunction in presymptomatic Huntington's Disease. Am J Neuroradiol. 2004; 25:1715–21. [PubMed: 15569736]

Pavese N, Andrews TC, Brooks DJ, Ho AK, Rosser AE, Barker RA, et al. Progressive striatal and cortical dopamine receptor dysfunction in Huntington's disease: a PET study. Brain. 2003; 126:1127–35. [PubMed: 12690052]

Pavese N, Gerhard A, Tai YF, Ho AK, Turkheimer F, Barker RA, et al. Microglial activation correlates with severity in Huntington disease: a clinical and PET study. Neurology. 2006; 66:1638–43. [PubMed: 16769933]

Reading SA, Dziorny AC, Peroutka LA, Schreiber M, Gourley LM, Yallapragada V, et al. Functional brain changes in presymptomatic Huntington's disease. Ann Neurol. 2004; 55:879–83. [PubMed: 15174024]

Rosas HD, Feigin AS, Hersch SM. Using advances in neuroimaging to detect, understand, and monitor disease progression in Huntington's disease. Neuro Rx. 2004; 1:263–72.

Rosas HD, Liu AK, Hersch S, Glessner M, Ferrante RJ, Salat DH, et al. Regional and progressive thinning of the cortical ribbon in Huntington's disease. Neurology. 2002; 58:695–701. [PubMed: 11889230]

Ross CA, Aylward EH, Stout JC, Biglan KM, Hayden MR, Shoulson I, et al. Clinical and radiographic features among presymptomatic individuals carrying an expanded CAG repeat in the Huntington's disease gene: analysis of baseline characteristics of the PREDICT-HD Cohort. Neurology. 2004; 62:A357.

Saft C, Zange J, Andrich J, Muller K, Lindenberg K, Landwehrmeyer B, et al. Mitochondrial impairment in patients and asymptomatic mutation carriers of Huntington's disease. Mov Disord. 2005; 20:674–9. [PubMed: 15704211]

Sandford, J.; Turner, A. Intermediate visual and auditory (IVA). Richmond: Brain Train; 1995.

Schmahmann, JD.; Doyon, J.; Toga, AW.; Petrides, M.; Evans, AC. MRI atlas of the human cerebellum. San Diego: Academic Press; 2000.

Searle, SS.; Casella, G.; McCulloch, CE. Variance components. New York: John Wiley & Sons; 1992.

Singer JD. Using SAS PROC MIXED to fit multilevel models, hierarchical models, and individual growth models. J Edu Behav Stat. 1998; 25:323–55.

Singer, JD.; Willett, JB. Applied longitudinal data analysis: modeling change and event occurrence. New York: Oxford University Press; 2003.

Smith, A. Symbol Digit Modalities Test (SDMT) manual (revised). Los Angeles: Western Psychological Services; 1982.

Smith Y, Raju DV, Pare JF, Sidibe M. The thalamostriatal system: a highly specific network of the basal ganglia circuitry. Trends Neurosci. 2004; 27:520–7. [PubMed: 15331233]

Sotrel A, Paskevich PA, Kiely DK, Bird ED, Williams RS, Myers RH. Morphometric analysis of the prefrontal cortex in Huntington's disease. Neurology. 1991; 41:1117–23. [PubMed: 1829794]

Spetsieris P, Ma Y, Dhawan V, Moeller JR, Eidelberg D. Highly automated computer-aided diagnosis of neurological disorders using functional brain imaging. Proc SPIE: medical imaging. 2006; 6144:61445-M1–12.

Tabrizi SJ, Cleeter MW, Xuereb J, Taanman JW, Cooper JM, Schapira AH. Biochemical abnormalities and excitotoxicity in Huntington's disease brain. Ann Neurol. 1999; 45:25–32. [PubMed: 9894873]

Takikawa S, Dhawan V, Spetsieris P, Robeson W, Chaly T, Dahl R, et al. Noninvasive quantitative fluorodeoxyglucose PET studies with an estimated input function derived from a population-based arterial blood curve. Radiology. 1993; 188:131–6. [PubMed: 8511286]

Trošt M, Carbon M, Edwards C, Raymond D, Mentis M, Moeller JR, et al. Primary dystonia: is abnormal functional brain architecture linked to genotype? Ann Neurol. 2002; 52:853–6. [PubMed: 12447944]

Underwood BR, Broadhurst D, Dunn WB, Ellis DI, Michell AW, Vacher C, et al. Huntington disease patients and transgenic mice have similar pro-catabolic serum metabolite profiles. Brain. 2006; 129:877–86. [PubMed: 16464959]

van Oostrom JC, Maguire RP, Verschuuren-Bemelmans CC, Veenma-van der DL, Pruim J, Roos RA, et al. Striatal dopamine D2 receptors, metabolism, and volume in preclinical Huntington disease. Neurology. 2005; 65:941–3. [PubMed: 16186542]

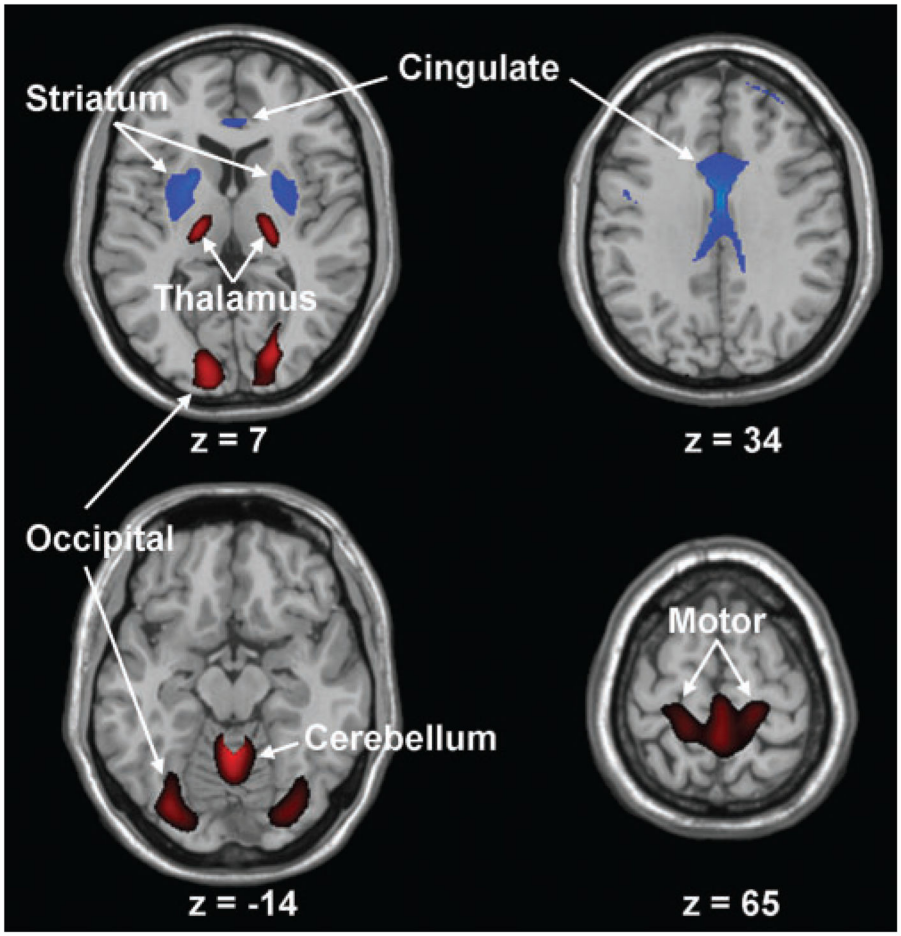

Fig. 1.

Huntington's disease-related pattern. This spatial covariance pattern was identified by network analysis of baseline FDG PET scans from 12 p-HD gene carriers and 12 age-matched healthy volunteer subjects. This pattern, representing the PC1 in the combined group analysis, accounted for 18% of the subject × voxel variation. Subject scores for this HD-related pattern (HDRP), representing network expression in individual subjects, discriminated the p-HD subjects from the controls ($P<0.01$). The HDRP is characterized by relative metabolic decreases in the striatum and cingulate cortex, associated with relative increases in the ventral thalamus, motor cortex (BA 4) and occipital lobe (BA17, 18). [The display represents voxels that contribute significantly to the network at $P=0.005$ and that were demonstrated to be reliable by bootstrap resampling procedures [inverse coefficient of variation (ICV)>3.5; $P<0.001$].Voxels with positive region weights (metabolic increases) are colour coded from red to yellow; those with negative region weights (metabolic decreases) are colour coded from blue to purple. The numbers under each slice are in millimeters, relative to the anterior-posterior commissure line.]

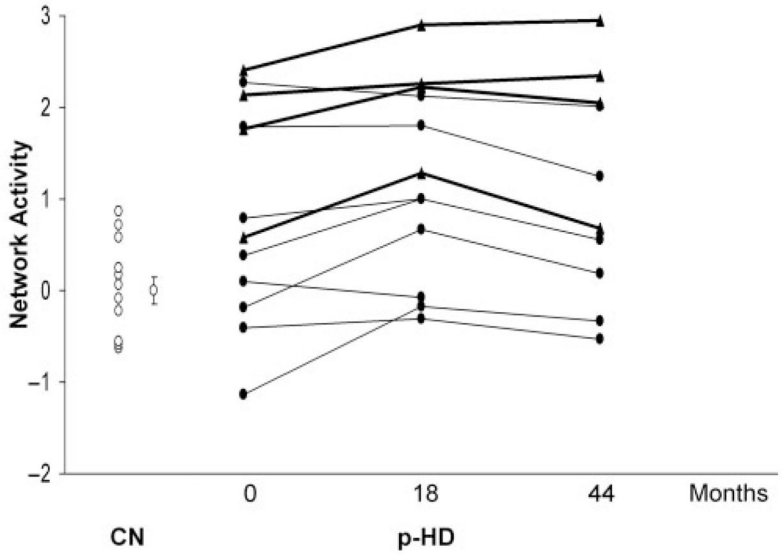

Fig. 2.

Changes in HDRP expression. Individual subject HDRP expression for the 12 p-HD subjects scanned at baseline, and following 18 and 44 months. Network activity is represented separately for the four p-HD subjects (filled triangles) who subsequently developed symptoms (bold lines), and for the eight remaining p-HD subjects (filled circles) who had not phenoconverted by the third time point (fine lines, see text). Values for 12 age-matched healthy control subjects (CN, open circles) are presented for reference. [Bar represents the SE of the control values.]

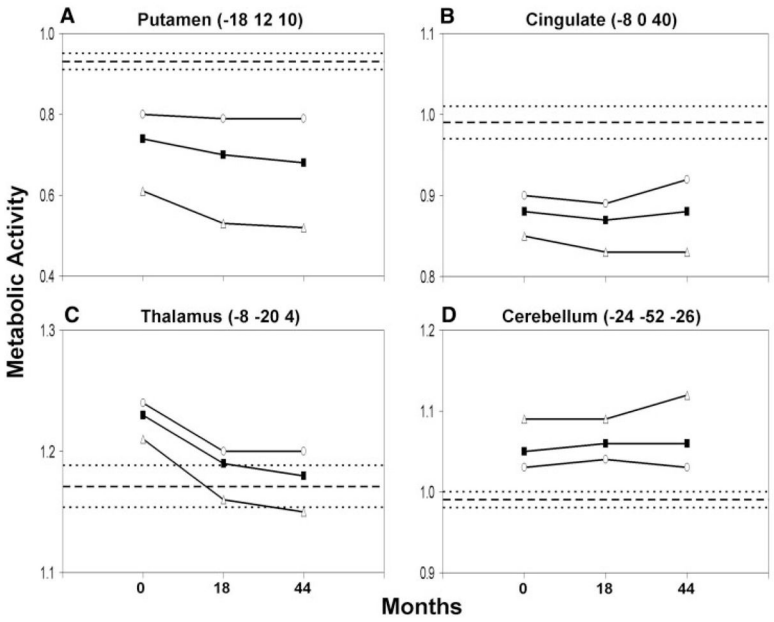

Fig. 3.

Regional glucose metabolism measured at representative nodes of the HDRP network. (**A**, **B**) In the striatum (putamen represented) normalized glucose metabolism declined over time ($P<0.005$). Significant reductions in striatal (putamen represented) metabolism are present at the baseline and follow-up PET visits in the p-HD cohort (filled squares). These reductions were comparatively greater in the p-HD subgroup who subsequently phenoconverted (open triangles). Regional glucose utilization was also reduced in the cingulate cortex throughout the period of observation. However, metabolism in this region did not change significantly over time. (**C**, **D**) In the thalamus (mediodorsal nucleus represented), normalized glucose utilization declined over time ($P<0.01$). In this region, baseline metabolic activity was abnormally elevated, particularly in the subgroup of gene carriers who did not phenoconvert during the course of the study (open circles). Although thalamic metabolism was also elevated at baseline in the subjects who subsequently phenoconverted (open triangles), metabolic activity in this region fell to normal levels as clinical signs emerged. By contrast, in the cerebellar vermis, metabolism was also elevated, but did not change over time. [The mean (±SE) for the 12 healthy control subjects is represented by broken lines.]

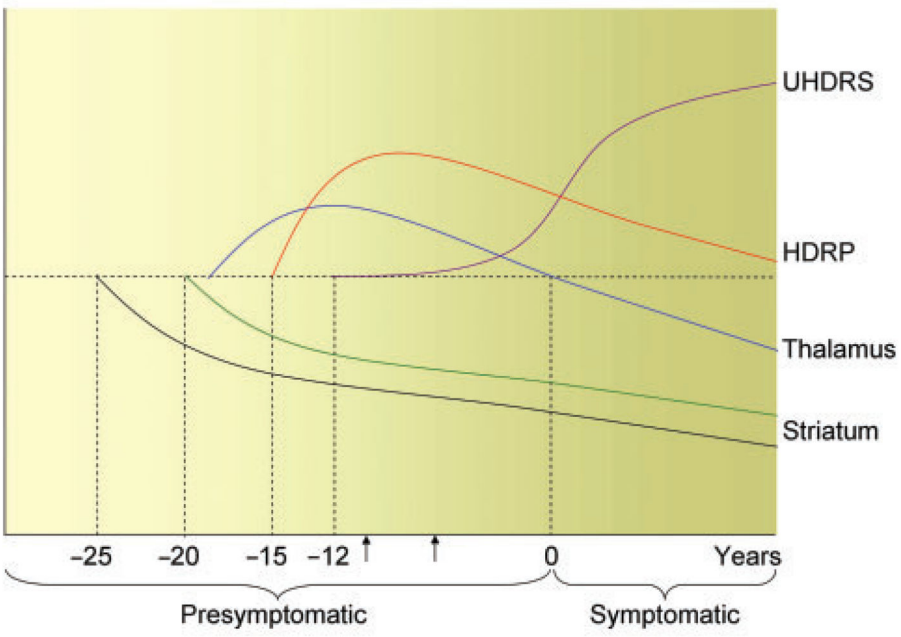

Fig. 4.

Hypothesized time course of changes in striatal D_2 binding, metabolic activity and clinical ratings in preclinical Huntington's disease. We used regression analysis of the data to estimate the time of onset (in years) of these functional changes prior to HD diagnosis (zero). Our data suggest that a decline in striatal D2 receptor binding (*black*) begins approximately 25 years before diagnosis. About five years later, striatal metabolism (*green*), an index of local neuronal viability, begins to fall. To compensate for striatal cell loss, thalamic metabolism (*blue*) increases (exactly when remains unknown) and with it, HDRP network activity (*red*). The latter measure peaks approximately 9 years before diagnosis. As thalamic metabolism declines, subtle clinical signs of disease (UHDRS, *purple*) emerge, beginning approximately 12 years before diagnosis. Concurrently, HDRP expression also falls, although remaining at supranormal levels (Feigin *et al*., 2001). The horizontal dashed line represents the normal mean. The arrows represent the estimated period of time of the current study.

Table 1

Brain regions with significant contributions to the Huntington's disease-related spatial covariance pattern (HDRP)

Brain region	Coordinates[a]			
	x	*y*	*z*	Z_{max}
Metabolic decreases				
Striatum, putamen left**	−22	0	8	3.55
right***	20	10	4	4.27
Cingulate gyrus, BA 23/24/32***	−2	16	28	4.05
	2	−22	30	3.91
Metabolic increases				
Thalamus, VL/VPL left**	−16	−18	4	3.01
right*	22	−20	6	2.78
Paracentral lobule, BA 4/6**	2	−42	68	3.13
Cerebellar vermis, Lobule IV-V[b]***	0	−52	−12	4.19
Lobule VIIB	6	−82	−30	2.98
Occipital lobe, BA18/19**	28	−80	−8	3.78

[a] Montreal Neurological Institute (MNI) standard space (Collins *et al*., 1994).

[b] According to Atlas of Schmahmann (Schmahmann *et al*., 2000).

* $P<0.01$;

** $P<0.005$;

*** $P<0.001$ (significance of correlations between normalized metabolism at peak voxel and whole-brain HDRP activity; see text).

Table 2

Network expression and regional metabolism in preclinical Huntington's disease

	Gene carriers			Controls
	Baseline	18 Months	44 Months	
Network expression[a]	0.88± 0.34	1.22±0.31	1.12±0.38	0.00± 0.15
Subgroup (1)	1.73±0.40	2.17±0.33	2.01±0.48	
(2)	0.45± 0.40	0.75± 0.32	0.52±0.34	
Regional metabolism[b]				
Putamen	0.74± 0.05	0.70± 0.05	0.68± 0.07	0.93±0.02
Subgroup (1)	0.61±0.06	0.53±0.07	0.52±0.08	
(2)	0.80± 0.05	0.79± 0.05	0.79± 0.07	
Cingulate cortex	0.88± 0.01	0.8± 0.01	0.88± 0.02	0.99± 0.02
Subgroup (1)	0.85± 0.02	0.83±0.03	0.83±0.04	
(2)	0.90± 0.01	0.89± 0.01	0.92±0.02	
Thalamus	1.23±0.01	1.19± 0.01	1.18± 0.01	1.17±0.02
Subgroup (1)	1.21±0.02	1.16± 0.02	1.15± 0.02	
(2)	1.24± 0.02	1.20± 0.02	1.20± 0.02	
Cerebellum	1.05± 0.01	1.06± 0.02	1.06± 0.02	0.99± 0.01
Subgroup (1)	1.09± 0.01	1.09± 0.02	1.12±0.01	
(2)	1.03±0.01	1.04± 0.02	1.03±0.02	

Subgroup (1): Preclinical HD subjects (n =4) who phenoconverted during the follow-up period.

Subgroup (2): Preclinical HD subjects (n =8) who at follow-up remained in the preclinical phase of the disease.

[a] HDRP expression (mean score ± SE).

[b] Globally normalized regional metabolic rate for glucose (mean ± SE).